Silicon-organic hybrid (SOH) IQ modulator using the linear electro-optic effect for transmitting 16QAM at 112 Gbit/s

Dietmar Korn,[1,*] Robert Palmer,[1] Hui Yu,[2] Philipp C. Schindler,[1] Luca Alloatti,[1] Moritz Baier,[1] René Schmogrow,[1] Wim Bogaerts,[2] Shankar Kumar Selvaraja,[2] Guy Lepage,[3] Marianna Pantouvaki,[3] Johan M.D. Wouters,[3] Peter Verheyen,[3] Joris Van Campenhout,[3] Baoquan Chen,[4] Roel Baets,[2] Philippe Absil,[3] Raluca Dinu,[4] Christian Koos,[1] Wolfgang Freude,[1] and Juerg Leuthold[1,5]

[1]Karlsruhe Institute of Technology (KIT), Institutes IPQ and IMT, Karlsruhe, Germany
[2]Photonics Research Group, Ghent University – IMEC, Department of Information Technology, Gent, Belgium
[3]IMEC, Leuven, Belgium
[4]GigOptix Inc., Bothell (WA), USA
[5]Now with ETH-Zurich, Zurich, Switzerland
[*]korn@kit.edu

Abstract: Advanced modulation formats call for suitable IQ modulators. Using the silicon-on-insulator (SOI) platform we exploit the linear electro-optic effect by functionalizing a photonic integrated circuit with an organic $\chi^{(2)}$-nonlinear cladding. We demonstrate that this silicon-organic hybrid (SOH) technology allows the fabrication of IQ modulators for generating 16QAM signals with data rates up to 112 Gbit/s. To the best of our knowledge, this is the highest single-polarization data rate achieved so far with a silicon-integrated modulator. We found an energy consumption of 640 fJ/bit.

OCIS codes: (250.7360) Waveguide modulators; (060.4080) Modulation; (230.7370) Waveguides; (250.5300) Photonic integrated circuits.

References and links

1. W. M. Green, M. J. Rooks, L. Sekaric, and Y. A. Vlasov, "Ultra-compact, low RF power, 10 Gb/s silicon Mach-Zehnder modulator," Opt. Express **15**(25), 17106–17113 (2007).
2. L. Liao, A. Liu, D. Rubin, J. Basak, Y. Chetrit, H. Nguyen, R. Cohen, N. Izhaky, and M. Paniccia, "40 Gbit/s silicon optical modulator for high-speed applications," Electron. Lett. **43**(22), 1196–1197 (2007).
3. A. Brimont, D. J. Thomson, P. Sanchis, J. Herrera, F. Y. Gardes, J. M. Fedeli, G. T. Reed, and J. Martí, "High speed silicon electro-optical modulators enhanced via slow light propagation," Opt. Express **19**(21), 20876–20885 (2011).
4. J. H. Wülbern, J. Hampe, A. Petrov, M. Eich, J. Luo, A. K.-Y. Jen, A. Di Falco, T. F. Krauss, and J. Bruns, "Electro-optic modulation in slotted resonant photonic crystal heterostructures," Appl. Phys. Lett. **94**(24), 241107 (2009).
5. K. Padmaraju, N. Ophir, Q. Xu, B. Schmidt, J. Shakya, S. Manipatruni, M. Lipson, and K. Bergman, "Error-free transmission of microring-modulated BPSK," Opt. Express **20**(8), 8681–8688 (2012).
6. P. Dong, C. Xie, L. Chen, N. K. Fontaine, and Y. K. Chen, "Experimental demonstration of microring quadrature phase-shift keying modulators," Opt. Lett. **37**(7), 1178–1180 (2012).
7. H. Yu, M. Pantouvaki, J. Van Campenhout, D. Korn, K. Komorowska, P. Dumon, Y. Li, P. Verheyen, P. Absil, L. Alloatti, D. Hillerkuss, J. Leuthold, R. Baets, and W. Bogaerts, "Performance tradeoff between lateral and interdigitated doping patterns for high speed carrier-depletion based silicon modulators," Opt. Express **20**(12), 12926–12938 (2012).
8. D. J. Thomson, F. Y. Gardes, J.-M. Fedeli, S. Zlatanovic, Y. Hu, B. P. P. Kuo, E. Myslivets, N. Alic, S. Radic, G. Z. Mashanovich, and G. T. Reed, "50-Gb/s silicon optical modulator," IEEE Photon. Technol. Lett. **24**(4), 234–236 (2012).
9. L. Alloatti, D. Korn, R. Palmer, D. Hillerkuss, J. Li, A. Barklund, R. Dinu, J. Wieland, M. Fournier, J. Fedeli, H. Yu, W. Bogaerts, P. Dumon, R. Baets, C. Koos, W. Freude, and J. Leuthold, "42.7 Gbit/s electro-optic modulator in silicon technology," Opt. Express **19**(12), 11841–11851 (2011).
10. P. Dong, C. Xie, L. Chen, L. L. Buhl, and Y.-K. Chen, "112-Gb/s monolithic PDM-QPSK modulator in silicon," Opt. Express **20**(26), B624–B629 (2012).

11. R. S. Jacobsen, K. N. Andersen, P. I. Borel, J. Fage-Pedersen, L. H. Frandsen, O. Hansen, M. Kristensen, A. V. Lavrinenko, G. Moulin, H. Ou, C. Peucheret, B. Zsigri, and A. Bjarklev, "Strained silicon as a new electro-optic material," Nature **441**(7090), 199–202 (2006).
12. B. Chmielak, M. Waldow, C. Matheisen, C. Ripperda, J. Bolten, T. Wahlbrink, M. Nagel, F. Merget, and H. Kurz, "Pockels effect based fully integrated, strained silicon electro-optic modulator," Opt. Express **19**(18), 17212–17219 (2011).
13. T. Baehr-Jones, M. Hochberg, G. Wang, R. Lawson, Y. Liao, P. Sullivan, L. Dalton, A. Jen, and A. Scherer, "Optical modulation and detection in slotted Silicon waveguides," Opt. Express **13**(14), 5216–5226 (2005).
14. J.-M. Brosi, C. Koos, L. C. Andreani, M. Waldow, J. Leuthold, and W. Freude, "High-speed low-voltage electro-optic modulator with a polymer-infiltrated silicon photonic crystal waveguide," Opt. Express **16**(6), 4177–4191 (2008).
15. J. H. Wülbern, A. Petrov, and M. Eich, "Electro-optical modulator in a polymer-infiltrated silicon slotted photonic crystal waveguide heterostructure resonator," Opt. Express **17**(1), 304–313 (2009).
16. I. Young, E. Mohammed, J. S. Liao, A. Kern, S. Palermo, B. Block, M. Reshotko, and P. D. Chang, "Optical technology for energy efficient I/O in high performance computing," IEEE Commun. Mag. **48**(10), 184–191 (2010).
17. R. Palmer, L. Alloatti, D. Korn, P. C. Schindler, M. Baier, J. Bolten, T. Wahlbrink, M. Waldow, R. Dinu, W. Freude, C. Koos, and J. Leuthold, "Low power Mach-Zehnder modulator in Silicon-Organic Hybrid Technology," IEEE Photonics Technology Letters, 10.1109/LPT.2013.2260858 (2013).
18. P. Dong, L. Chen, and Y. K. Chen, "High-speed low-voltage single-drive push-pull silicon Mach-Zehnder modulators," Opt. Express **20**(6), 6163–6169 (2012).
19. A. Brimont, D. J. Thomson, F. Y. Gardes, J. M. Fedeli, G. T. Reed, J. Martí, and P. Sanchis, "High-contrast 40 Gb/s operation of a 500 µm long silicon carrier-depletion slow wave modulator," Opt. Lett. **37**(17), 3504–3506 (2012).
20. J. Witzens, T. Baehr-Jones, and M. Hochberg, "Design of transmission line driven slot waveguide Mach-Zehnder interferometers and application to analog optical links," Opt. Express **18**(16), 16902–16928 (2010).
21. F. Van Laere, T. Claes, J. Schrauwen, S. Scheerlinck, W. Bogaerts, D. Taillaert, L. O'Faolain, D. Van Thourhout, and R. Baets, "Compact focusing grating couplers for silicon-on-insulator integrated circuits," IEEE Photon. Technol. Lett. **19**(23), 1919–1921 (2007).
22. W. Bogaerts and S. K. Selvaraja, "Compact single-mode silicon hybrid rib/strip waveguide with adiabatic bends," IEEE Photon. J. **3**(3), 422–432 (2011).
23. D. Jin, H. Chen, A. Barklund, J. Mallari, G. Yu, E. Miller, and R. Dinu, "EO polymer modulators reliability study," Proc. SPIE **7599**, 75990H (2010).
24. H. Chen, B. Chen, D. Huang, D. Jin, J. D. Luo, A. K.-Y. Jen, and R. Dinu, "Broadband electro-optic polymer modulators with high electro-optic activity and low poling induced optical loss," Appl. Phys. Lett. **93**(4), 043507 (2008).
25. R. Blum, M. Sprave, J. Sablotny, and M. Eich, "High-electric-field poling of nonlinear optical polymers," J. Opt. Soc. Am. B **15**(1), 318–328 (1998).
26. R. Palmer, L. Alloatti, D. Korn, W. Heni, P. C. Schindler, J. Bolten, M. Karl, M. Waldow, T. Wahlbrink, W. Freude, C. Koos, and J. Leuthold, "Low-loss silicon strip-to-slot mode converters," IEEE Photonics Journal **5**(1), 2200409 (2013).
27. R. Schmogrow, D. Hillerkuss, M. Dreschmann, M. Huebner, M. Winter, J. Meyer, B. Nebendahl, C. Koos, J. Becker, W. Freude, and J. Leuthold, "Real-time software-defined multiformat transmitter generating 64QAM at 28 GBd," IEEE Photon. Technol. Lett. **22**(21), 1601–1603 (2010).
28. R. Palmer, L. Alloatti, D. Korn, P. C. Schindler, R. Schmogrow, W. Heni, S. Koenig, J. Bolten, T. Wahlbrink, M. Waldow, H. Yu, W. Bogaerts, P. Verheyen, G. Lepage, M. Pantouvaki, J. Van Campenhout, P. Absil, R. Dinu, W. Freude, C. Koos, and J. Leuthold, "Silicon-organic hybrid MZI modulator generating OOK, BPSK and 8-ASK signals for up to 84 Gbit/s," IEEE Photonics Journal **5**, 6600907–6600907 (2013).
29. R. Schmogrow, B. Nebendahl, M. Winter, A. Josten, D. Hillerkuss, S. Koenig, J. Meyer, M. Dreschmann, M. Huebner, C. Koos, J. Becker, W. Freude, and J. Leuthold, "Error vector magnitude as a performance measure for advanced modulation formats," IEEE Photonics Technology Letters **24**, 61–63 (2012). Correction: *ibid.*, **24**, 2198 (2012).
30. J. Proakis and M. Salehi, *Digital Communications,* 3rd Ed. (McGraw-Hill Education 1995). Section 4–3-1.
31. L. Dalton and S. Benight, "Theory-guided design of organic electro-optic materials and devices," Polymers **3**(4), 1325–1351 (2011).
32. D. Hillerkuss, R. Schmogrow, T. Schellinger, M. Jordan, M. Winter, G. Huber, T. Vallaitis, R. Bonk, P. Kleinow, F. Frey, M. Roeger, S. Koenig, A. Ludwig, A. Marculescu, J. Li, M. Hoh, M. Dreschmann, J. Meyer, S. B. Ezra, N. Narkiss, B. Nebendahl, F. Parmigiani, P. Petropoulos, B. Resan, A. Oehler, K. Weingarten, T. Ellermeyer, J. Lutz, M. Moeller, M. Huebner, J. Becker, C. Koos, W. Freude, and J. Leuthold, "26 Tbit s-1 line-rate super-channel transmission utilizing all-optical fast Fourier transform processing," Nat. Photonics **5**(6), 364–371 (2011).

1. Introduction

Modulators that can reliably access any point within a constellation diagram are needed to encode signals with advanced modulation formats. The realization of these key components as photonic integrated circuits (PIC) on the silicon-on-insulator (SOI) platform holds promise

for low power consumption, low cost and high volume production. Currently, LiNbO$_3$-based modulators are used for the most part. Exploiting the established infrastructure from scalable CMOS technology a new generation of silicon photonic devices emerges and is likely to substitute LiNbO$_3$, especially when arrays of modulators will be needed.

CMOS process compatibility for fabrication is essential to further silicon photonic modulators. A common approach is to confine the production of SOI modulators to a few simple steps such as silicon etching, doping & annealing, deposition of dielectric layers and metal electrodes. And indeed, the most common silicon modulators that are based on a pin or pn junction within a silicon ridge waveguide rely on these CMOS process steps. In these modulators free-carrier dispersion is employed by injecting [1] or depleting [2] carriers. This gives control over the phase of light, but also changes the absorption, which makes arbitrary waveform generation intricate. So far, numerous silicon modulators using this principle have been demonstrated in resonant configurations [3–6]. Also non-resonant designs [7] were published showing an attractive bandwidth for on-off-keying (OOK) at data rates up to 50 Gbit/s [8]. While an increase in modulation bandwidth seems certainly possible [9], bandwidth limitations in electronics would favor advanced modulation formats with reduced symbol rates. That means going to complex modulation formats like quadrature-phase shift keying (QPSK) as shown at 28 GBd in [10] to transmit 56 Gbit/s in a single polarization is a more advanced way to increase the bit-rate. In addition, polarization multiplexing can be added to further double the bit-rate. In the aforementioned publication [10] it has recently been shown how polarization multiplexing can be realized on-chip.

CMOS compatibility also sets limits to the available voltages. In light of rather high reverse bias and RF voltages reported for high-speed implementations (with respect to achievable phase shifts in silicon) it is advisable to also consider the linear electro-optic (Pockels) effect. The linear electro-optic effect can be found in strained silicon [11,12]. Alternatively, the very common technique of spin-coating can be used to add an electro-optic, $\chi^{(2)}$-nonlinear organic cover layer on the modulator waveguide [13–16] in order to create a silicon-organic hybrid (SOH) device. Applying a voltage then results in an instantaneous, pure phase shift, exactly as in LiNbO$_3$. This is an advantage over free-carrier based plasma effect modulation, where phase and amplitude modulation are linked. The free choice of cover material brings the potential to reduce currently reported voltage-length-products for high-speed modulation to 3.8 Vmm (at 10 Gbit/s) [17] or even lower for future advanced nonlinear organic materials, while pn-modulators so far show $V_\pi L \geq 10$ Vmm [18] (8.5 Vmm at 40 Gbit/s for a resonant structure [19]). The SOH approach combines the advantages of silicon (fabless development, fabrication infrastructure, scalability to high volume production) with the strong $\chi^{(2)}$-nonlinearity of an organic material.

In this paper we demonstrate the first IQ modulator for advanced modulation formats on the SOI-platform which is suited to transmit multilevel phase and amplitude encoded signals in the C-band. By applying the SOH concept, our approach with pure phase modulators in an interferometer structure gives us the freedom to choose any constellation, and enables arbitrary signal generation. Because of its relevance in applications, we decided for a 16QAM format for demonstrating the so far highest single-carrier single-polarization data rate of 112 Gbit/s on the silicon-platform. We further show error free generation and reception of a QPSK signal at 56 Gbit/s.

2. Structure of the silicon-organic hybrid IQ modulator

The IQ modulator is constructed by nesting two Mach-Zehnder modulators (MZMs) as shown in Fig. 1(a). These single-drive modulators are operated in push-pull mode at minimum transmission point, such that the resulting amplitude modulation of each provides the in-phase (I) and quadrature-(Q) phase component, when both MZMs are made to interfere with a phase shift of $\pi/2$.

To explain the SOH modulator concept a cross section of one MZM is presented in a simplified manner in Fig. 1(b). Light propagates in the two slot waveguides (WG) shown in

blue. They constitute the arms of the MZM and are filled with the nonlinear material. The large index contrast between Si of n_{Si} = 3.48 and the nonlinear polymer n_{poly} = 1.7 causes an enhancement of the electrical field of the optical quasi-TE wave inside the slot, see Fig. 1(c). When a voltage is applied to the Si rails, it creates a strong electric field across the slot, see Fig. 1(d). Thus a large and therefore efficient overlap is obtained between the electrical and optical mode. By attaching thin Si striploads to the optical WG an electrical connection is made to an RF coplanar waveguide (CPW), realized in a ground-signal-ground (GSG) configuration devised to have a 50 Ω impedance close to the RF source (similar to [20]). The active molecules (chromophores) of the nonlinear material are aligned during fabrication by applying a poling voltage (depicted in green) from one ground electrode to the next, which results in an orientation of the $\chi^{(2)}$ nonlinearity in both slots (green arrows) that is asymmetric with respect to the signal electrode (S). Thus in operation, when an RF signal on the S-electrode is applied, it will cause a positive phase shift in one arm and a negative one in the other, i.e., result in push-pull operation. Thus the MZM can deliver a pure amplitude modulation.
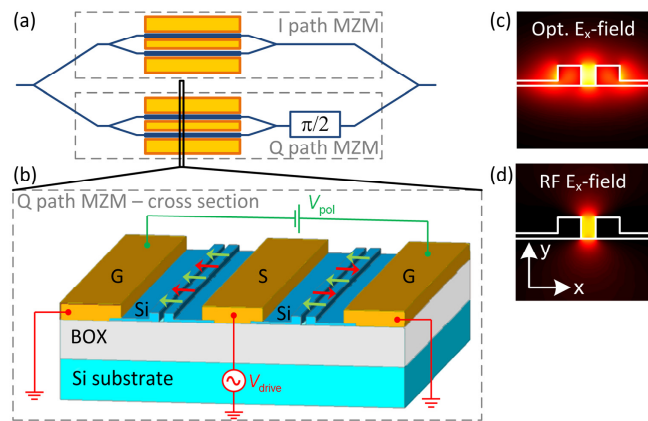

Fig. 1. IQ modulator based on the SOH concept. (a) Topview of the IQ modulator with nested Mach-Zehnder modulators (MZM), displaying optical waveguides (WG) in blue and electrical lines in orange. (b) Cross section of an SOH MZM, showing two silicon striploaded slot WGs, which act as phase shifters. They are filled and covered with a nonlinear cladding (not shown for clarity). The coplanar RF transmission line (GSG, ground-signal-ground) is impedance matched to the driving signal generator. The RF voltage at the S-electrode creates oppositely directed electric slot fields (red arrows). During the fabrication process, the χ(2)-nonlinearity is created by applying a poling voltage between both RF ground (G) electrodes at an elevated temperature. This aligns (poles) the active cladding molecules in a direction indicated by green arrows. In combination with the poled cladding, the modulating RF voltage leads to opposite phase shifts in both interferometer arms. (c) Color-coded dominant x-component |Ex| of the optical electrical field in the slot WG cross section. (d) Modulating electrical RF field. Both fields are strongly confined to the slot, resulting in high modulation efficiency.

Our implementation of the MZM is depicted as a detailed cross section in Fig. 2. We start at IMEC with an SOI wafer (SOITEC). It has a 220 nm high waveguide (WG) layer on a 2 µm thick buried oxide (BOX). Using 193 nm deep UV lithography slot WGs (w_{Slot} = 140 nm, w_{Rail} = 220 nm, h_{Rail} = 220 nm) with n-doped silicon striploads ($h_{Stripload}$ = 50 nm, As-doping with nominally 3×10^{17} cm^{-3}) are etched into the WG layer. Furthermore dry etching is employed to remove 70 nm of Si for standard grating couplers [21] and standard strip and rib WGs for low loss access waveguides [22].

A silicide film (surrounded by highly doped silicon with nominally 1×10^{20} cm^{-3}) connects through tungsten-filled (W) vias to the copper electrodes of the RF transmission line. Using this CMOS-like metal stack a conducting connection between the RF transmission lines (guiding the electrical modulating wave) and the rails (guiding the optical field) is established. It allows crossings of optical WGs with electrical transmission lines, where the

surrounding dielectric layers of mostly SiO_2 and Si_3N_4 fix the distance to $d_{Cu\text{-}BOX} = 1.1$ µm. This metal stack is ready to be extended with additional standard layers, e.g. to make aluminum pads for packaging. We finished this metal stack with a thin layer of SiC to protect the Cu from air for this proof-of-principle device.

To transform the 1.5 mm long slot WGs into active modulator sections, trenches are etched into the dielectric layers to expose the slot WGs by a combination of dry and wet etching. A commercially available and reliable [23] electro-optic polymer is spin-coated. This material (named M3 by the supplier GigOptix Inc [24].) contains chromophores and is the very same material used in Telecordia certified polymer modulators of the same manufacturer. It is poled [25] inside the slot WG (alignment of the chromophores) by applying a DC voltage at elevated temperature to create the $\chi^{(2)}$ nonlinearity in the same way as in [9].
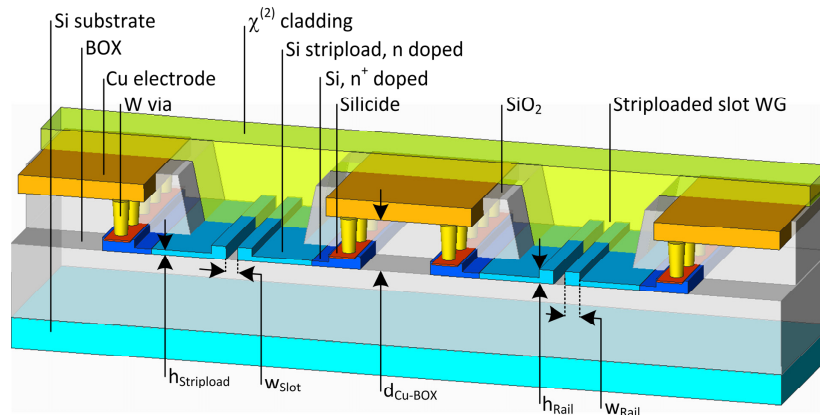

Fig. 2. Detailed cross section of MZM as implemented, showing two phase modulators with striploaded slot WGs, filled with nonlinear cladding; not to scale. Rails are connected to ground-signal-ground electrodes by tungsten vias, a silicide layer and the Si striploads. This electrode arrangement allows crossings of optical WGs and electrical transmission lines. Furthermore, it corresponds to the first part of standard metal stacks as known from CMOS technology.

The MZMs further consist of multi-mode interference (MMI) couplers. A transition from the slot WG to standard strip WGs is achieved by using a low-loss converter as described in [26]. These single-drive modulators are in turn nested within one large MZ interferometer with a path length imbalance of 40 µm. The I and Q path are operated each in push-pull with ground-signal-ground (GSG) electrodes, such that their operation points can be set by applying a bias voltage along with the RF signal. The phase difference between I- and Q-component can be controlled by changing the operation wavelength in this proof-of-principle PIC.

3. Demonstrations

The performance of the IQ modulator is determined by the properties of its nested MZMs. The electro-optic small signal frequency response S_{21} of one MZM which is operated at its quadrature point is shown in Fig. 3. The 45 GHz RF probes were not de-embedded. The modulated light output power is detected with a photodiode. The raw frequency response of $|S_{21}|$ is recorded with a vector network analyzer (VNA). When switching off the optical carrier, a noise floor from the optical detector is seen. The blue curves result from a moving average applied to the measured data (red dots). The inset shows a blow up of the averaged frequency response in the low-frequency region. The receiver's equalizer (red curve) compensates the overall frequency response (magenta curve). The gray vertical line at 0.9 GHz marks the reference for normalizing the response function. The horizontal grey lines

mark the −3 dB and −6 dB deviations from this reference point. The uncompensated −3 dB limiting frequency is 6.8 GHz, the −6 dB limit is 21 GHz.

This curve is atypical for a modulator insofar as the response drops sharply in a frequency range up to 1.7 GHz, see inset. Comparable curves were reported in Ref [9]. for a silicon modulator with a very similar EO polymer (M1) from GigOptix. The skin effect becomes more pronounced for higher frequencies; hence the RF loss increases strongly with frequency, especially for our relatively thin electrodes. A 3 dB bandwidth of 6.8 GHz results for this modulator. For higher frequencies the response flattens resulting in a 6 dB bandwidth of 21 GHz. The region with the sharp sensitivity increase toward lower frequencies does not significantly affect the transmission quality as demonstrated in our experiments. Line coding and forward error correction tend to avoid the lower spectral regions anyway. Instead of equalizing at the receiver (red curve in Fig. 3) as used for QPSK, we used a pre-emphasis for 16QAM in the transmitter. We keep the pre-emphasis filter length short, which means that it can be implemented as a lookup table in the transmitter driver electronics, which is available anyway for generating multi-level signals for higher order modulation formats.
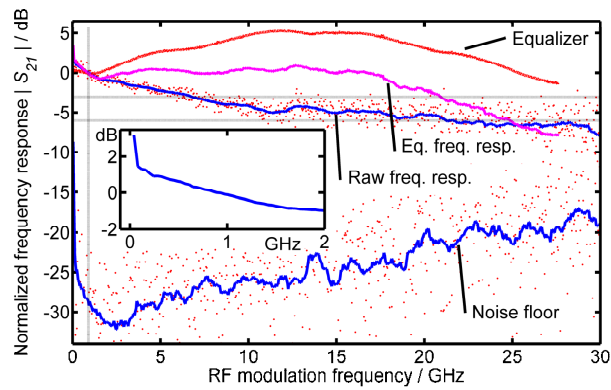

Fig. 3. Electro-optic frequency response S_{21} of our MZM (including the RF probes). The modulator is driven with a small-signal sinusoidal at the quadrature operating point. The modulated light output power is detected with a photodiode. The raw frequency response is recorded with a vector network analyzer (VNA). When switching off the optical carrier, a noise floor from the optical detector is seen. The blue curves result from a moving average applied to the measured data (red dots). The inset shows a blow up of the averaged frequency response in the low-frequency region. The receiver's equalizer (red curve) compensates the overall frequency response (magenta curve). The gray vertical line at 0.9 GHz marks the beginning of the frequency range which is of interest for data transmission (PRBS length 2^{31}-1). This frequency was chosen for normalizing the response function. The horizontal grey lines mark the −3 dB and −6 dB deviations from this reference point. The uncompensated −3 dB limiting frequency is 6.8 GHz, the −6 dB limit is 21 GHz.

To test data transmission with the SOH IQ modulator, two random signals with a pseudo-random binary sequence (PRBS) of length 2^{11}-1 have been created with an electrical arbitrary waveform generator (AWG) [27] at a symbol rate of 28 GBd (symbol duration is T_s = 35.7 ps). Our PRBS length was limited, but in [28] we checked that a PRBS length of 2^{31}-1 applied to a comparable modulator structure led to comparable bit-error ratios (BER). After amplification to a peak-to-peak driving voltage of 5 V and having added bias voltages (V_π = 2 V at DC) of 0 V to 4 V (MZMs set to minimum transmission point), the electrical signal is fed via RF probes to the chip and connected to off-chip 50 Ω terminations, as shown in Fig. 4. Light at 1545 nm is coupled with grating couplers (GC, >10 dB for both couplers), and modulated in amplitude and phase. Before reception with an optical modulation analyzer (OMA) for error detection, the modulated light is amplified, filtered and attenuated as needed. The same setup is also employed to investigate the dependence of BER on the optical signal-

to-noise ratio (OSNR) measured with an optical spectrum analyzer (OSA) while adding noise using an amplified spontaneous emission (ASE) source.

The device shows an extinction ratio of >26 dB. The measured overall optical insertion loss of 30 dB is high. However, we did not optimize all components for lowest loss. Our optical loss is composed of: (a) Coupling loss, which amounts to more than 10 dB for both grating couplers. Better grating couplers (with higher fabrication effort) promise coupling losses of 1.6 dB per coupler. (b) Loss in 7 mm long access WGs including bends and strip-to-ridge transitions (order of magnitude 5 dB/cm) by scattering (rough WG sidewalls) and absorption (WG partially located underneath metal). The access WG could have been shortened to 1 mm, but the excess length facilitated our experiments. (c) Concatenation of four MMIs. (d) Strip-to-slot transitions, each contributing 1 dB loss due to fabricating tolerances. (e) Phase modulator section is estimated to have a loss of 10.5 dB. Optimizing (a)–(d) would reduce the loss essentially to the loss of the phase modulator section.

We summarize the basic devices properties: The active modulator section is 1.5 mm long, contributes 10.5 dB optical loss, has a V_π of 2 V at DC, and exhibits a 3 dB (6 dB) bandwidth of 6.8 GHz (21 GHz). The extinction ratio is larger than 26 dB.
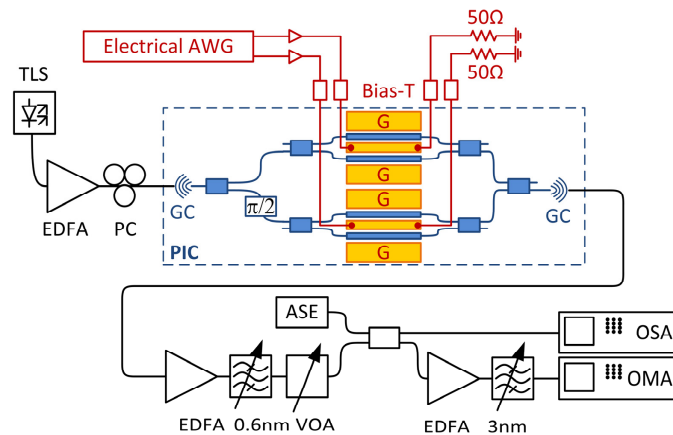

Fig. 4. Experimental setup with photonic integrated circuit (PIC) under test. In blue: Schematic SOI chip configuration with nested MZMs using MMIs, and with grating couplers (GC) to couple light at 1545 nm with cleaved standard single mode fibers (SSMF). In orange: Electric coplanar waveguides in ground-signal-ground (GSG) configuration contacted with RF probes to operate MZMs in push-pull mode. In red: Off-chip electrical components to supply the PRBS signal (electrical arbitrary waveform generator, AWG, electrical amplifier), bias-Ts (DC sources not shown) and termination. In black: Off-chip fiber based devices for characterization, including a tunable laser source (TLS), a polarization controller (PC), filters, erbium doped fiber amplifiers (EDFA), variable attenuator (VOA) and ASE source for OSNR tests.

QPSK, one of the most common formats used in coherent transmission systems is serving us as a benchmark. We can generate QPSK with the SOH modulators at a state-of-the-art symbol rate of 28 GBd, see Fig. 5. For the first time on the silicon platform we report, without relying on additional signal processing (such as pre-emphasis or equalization), a bit-error ratio (BER) of 4.5×10^{-4} for QPSK, i.e. well below the hard decision forward error correction threshold of 3×10^{-3}. The error vector magnitude (EVM, maximum normalization), a common measure for complex signals (directly related to the BER [29]), is 24.9% in this experiment. This measure provides a convenient tool for comparison with other, more advanced modulation formats, as used later. The imbalance between the I and Q path amounts to a factor of 1.3 and is due to unequal poling and imperfect adjustment of the operating points. By a careful adjustment of the I and Q voltages this imbalance can be compensated, and we did so for 16QAM.
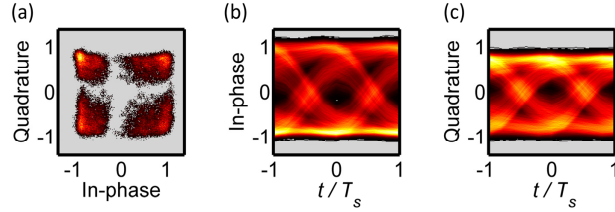
Fig. 5. QPSK generation at 56 Gbit/s with an IQ SOH modulator without using signal pre-emphasis, and detected without equalization. (a) Constellation and (b) in-phase and (c) quadrature-phase eye diagram. The BER is 4.5×10^{-4}, and the EVM is 24.9% and thus well below the FEC error correction limit.

Generation of error free QPSK with equalization (19 taps, 1 per symbol) is reported next, see Fig. 6, for the first time on the SOI platform at 28 GBd, also for direct comparison with [10] using the same equalizer length to reach 56 Gbit/s (the highest data rate reported on one channel and polarization). The EVM is 14.2 % and mostly due to the path imbalance. No errors could be found over minutes. The BER is plotted over OSNR showing direct BER measurements and EVM measurements translated to BER. This modulator is 5.5 dB from the theoretical limit of QPSK at a BER of 3×10^{-3}. It is conceivable that equalization could be integrated on-chip along with driver electronics, as one can save on forward error correction efforts in this case.
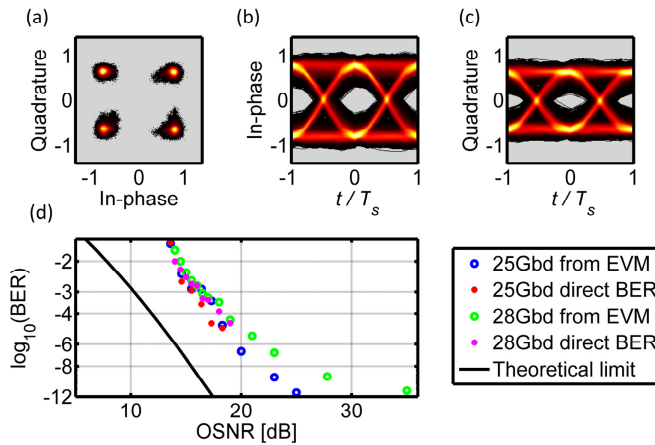

Fig. 6. QPSK generation at 56 Gbit/s with an IQ SOH modulator; detected using equalization with 19-taps as in [10]. Error free operation is measured and displayed in (a) constellation and (b, c) eye diagrams. The BER is shown in (d) in dependence of the OSNR at 25 GBd and 28 GBd. Measurements of the EVM are translated to BER and depicted.

16QAM is an advanced modulation format requiring complete control of amplitude and phase of the modulated signal. Using an 8-tap pre-emphasis, also correcting the IQ imbalance, the same modulator as above was used to generate an optical 16QAM signal at 28 GBd, i.e., 112 Gbit/s. This is currently the highest data rate on a single channel and polarization generated on the SOI platform, while still remaining below the FEC limit with a BER of 1.2×10^{-3}, an EVM of 10.3%, without any equalization at the receiver, see Fig. 7.
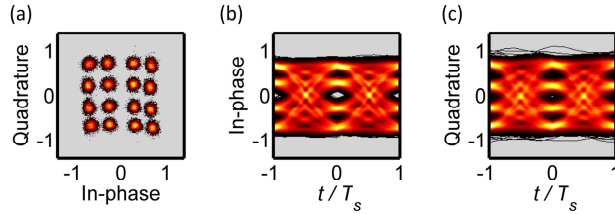
Fig. 7. Generation of 16QAM on a single channel and polarization at 112 Gbit/s with an IQ SOH modulator using pre-emphasis. (a) Constellation and (b, c) eye diagrams as observed when employing an 8-tap (1 tap per symbol) pre-emphasis at the transmitter, and no equalization at the receiver. The BER is 1.2×10^{-3}, and the EVM is 10.3%.

4. Discussion and conclusion

Advanced modulation formats not only bring higher spectral efficiency, but also a reduction of energy consumption of the modulator for a given driving voltage. Assuming a 50 Ω termination and a measured driving voltage of $V_{pp} = 5$ V (pre-emphasis reduces the effective voltage further, which is included in this estimation) we follow the recipe by [30] and find an energy consumption of 640 fJ/bit. Further improvements are to be expected when better nonlinear cladding materials are found [31] and, supposing driver electronics can be closely integrated, if the modulator's impedance can be designed to allow lower drive powers. Considering that an 8-tap pre-emphasis could be most easily implemented as a lookup table in the same electronics which generate the multi-level signal there is no demand for extra effort such as equalization.

This demonstration proves the potential of SOH modulators to compete with LiNbO₃ in its core domain of advanced modulation formats, and holds the promise for a reduction of cost, energy consumption, and size, in particular when making multichannel arrays. This extends the application range of silicon modulators further into long haul and access networks, which have been shown to strongly rely on ever more advanced modulation formats [32], while contending with symbol rates in a very similar range as the one used in this experiment.

Acknowledgments